

hysteresis effect for SMA actuator in trajectory tracking applications. Paper [5] introduced an inverse-Preisach model-based feedforward approach to compensate for dynamic and hysteresis effects in SMA with the application. However, the performance of the feed-forward controller depends on the accuracy hysteresis inverse model. In practice, the hysteresis model of the SMA actuator is sensitive to disturbances resulting in inaccurate estimation. Moreover, the feedforward control approach can not eliminate steady-state offset.

To overcome these drawbacks, hybrid feedforward control and feedback control are developed to improve the control quality. In [6], a hybrid control scheme which was composed of a feedforward controller based a hysteresis inverse Krasnosel'skii Pokrovskii model and a PID feedback controller was proposed to further improve the positioning accuracy of the SMA actuator. Paper [7] introduced a hybrid feedforward control based on the inverse Preisach model with the modified fuzzy sliding mode control which served as a feedback controller. Paper [8] introduced a novel control strategy combining a PID controller with an inverted hysteresis compensator using the Prandtl-Ishlinskii model. One major disadvantage of these methods was that the tracking performance of the SMA actuator highly relies on its inverse model. Besides, the physical constraints of the input voltage of the SMA actuator are hardly handled by the inversion-based method.

Recently, some studies used intelligent techniques to design an inverse compensation to cancel out the hysteretic effect and the proposed adaptive control law applied in the control process. Such as paper [9] introduced a position tracking control system for SMA actuator using neural network feedforward and robust integral of signum of error feedback. Paper [10] used a PID neural network to describe the hysteresis nonlinearity of the SMA actuator. Paper [11] presented a neural model predictive and variable structure controllers designed to control the rotary manipulator actuated by SMA. Paper [12] used a hybrid PID feedback with feedforward control based on an inverse generalized Prandtl-Ishlinskii model. And then, it is cascaded with an adaptive model reference temperature control to estimate the SMA electrical current for tracking the reference signal.

In summary, to improve the quality control of SMA actuator, two problems need to be considered that how to obtain the accurate approximation of a dynamic inversion compensator to cancel out the effect of the nonlinearities hysteresis and how to adaptive online control to adapt well to disturbances and dynamic variations in its operation. In this paper, a modified feedback error learning (MFEL) control is proposed. The ideas of this approach are as follows, first, a neural NARX model trained by a modified differential evolution algorithm [13] to design an inverse compensation of SMA actuator based on experimental data. To eliminate the steady state's error, a hybrid an inversion compensator combined with the PID feedback control is realized. And final, an adaptive back-propagation (aBP) with a self-adaptive learning rate based Sugeno Fuzzy logic to update online weighting values of a dynamic inversion compensator model as to adapt well to disturbances and dynamic variations in its operation. To prove the effectiveness of the proposed MFEL controller, first, the

benchmark nonlinear SISO system is used to evaluate the controller. Then, the experimental shape memory alloys (SMA) actuator is set up to test the controller.

2. Content

2.1. Original feedback error learning control

FEL controller was first proposed by Kawato [14] and the FEL scheme was described in Fig.1. The idea of the FEL scheme is to learn an inverse model or feedforward control by using the feedback control signal. If the feedback control signal goes to zero, then generally the error will also be zero.

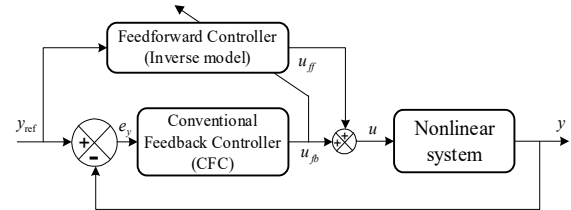


Fig.1 Block diagram of original FEL controller

In the FEL scheme, the CFC feedback control roles guarantee global asymptotic stability to the whole system. A stability of FEL controller was discussed by Miyamura et al. [15]. This stability proof was proved by lemma 1.

Lemma 1. Let $L(s)$ be a strongly positive real (SPR) transfer function and $\mathcal{E}(t)$ be an arbitrary time-varying vector. Then, the solution $z(t)$ of the differential equation

$$\frac{dz(t)}{dt} = -\mathcal{E}(t)L(s)\mathcal{E}(t)^T z(t) \quad (1)$$

tends to a constant vector z_0 such that $\mathcal{E}(t)z_0 \rightarrow 0$. If $\mathcal{E}(t)$ satisfies the so-called persistent excitation (PE) condition [16]. The above z_0 is equal to 0.

For a second order SISO systems, Nakanishi et al. [17] presented a Lyapunov analysis suggesting that the condition of SPR is a sufficient condition for asymptotic stability of the closedloop dynamics. The feedback gains must satisfy the condition $k_d^2 > k_p$ to guarantee the stability of FEL.

2.2. Modified feedback error learning control

This section presents a modified feedback error learning (MFEL) controller approach for nonlinear systems. The block diagram of the proposed controller is illustrated in Fig.2.

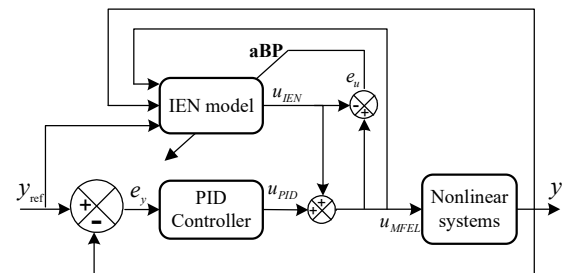


Fig.2 Block diagram of proposed MFEL controller

The basic idea of the proposed MFEL control consists of three steps. First, a neural NARX model trained modified differential evolution algorithm [13] is used for offline identifying a

dynamic inversion compensator to cancel out the effect of the nonlinearities feature. Then, a hybrid feedforward control combined with the PID feedback control is realized. Where the inverse evolutionary neural NARX (IEN) model provides a feedforward control signal from the desired trajectory. The PID controller is applied to improve the precision and reject the steady state's error in tracking control. And final, an adaptive back-propagation (aBP) with a self-adaptive learning rate based Sugeno Fuzzy system is developed and employed in the MFEL to adapt well to disturbances and dynamic variations in its operation. Based on Fig.2, the voltage control law is given by

$$u_{MFEL} = u_{PID} + u_{IEN} \quad (2)$$

Where u_{MFEL} is the control signal applied to the nonlinear system. The feedforward control signal u_{IEN} is provided by the IEN model and the control signal u_{PID} is produced by the PID controller based error $e_y = y_{REF} - y$ between reference position trajectory and position output. The PID controller output can be expressed as follows,

$$u_{PID}(t) = k_p e_y(t) + k_i \int_0^t e_y(\tau) d\tau + k_d \frac{de_y(t)}{dt} \quad (3)$$

And then, the weight values of the inversion compensator based IEN model are trained and adjusted online during real-time control by the feedback error control signal $e_u = u_{MFEL} - u_{IEN}$ to minimize the learning error defined as,

$$E_u = \frac{1}{2} (u_{MFEL} - u_{IEN})^2 = \frac{1}{2} u_{PID}^2 \quad (4)$$

2.2.1. Proposed IEN model

In practice, it is very difficult to identify the inverse dynamics of the system by using the mathematical method. In this part, the neural NARX model optimized by a modified differential evolution algorithm is used for identifying the inverse dynamic model based on the experimental input-output data. The block diagram of the IEN model is illustrated in Fig.3. The structure of the inverse neural NARX model and the details of the MDE training algorithm is described in [13].

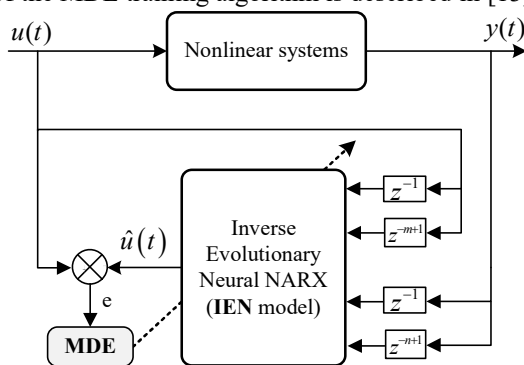


Fig.3 Block diagram of IEN model

2.2.2. An adaptive back-propagation (aBP) law

To adjust online the weight values of the inversion compensator based IEN model, an adaptive back-propagation (aBP) with self-adaptive learning rate based Sugeno Fuzzy logic is used to minimize E_u in Eq.(5) as below

$$\Delta w = w(new) - w(old) = -\lambda \frac{\partial E_u}{\partial w} \quad (5)$$

Using the chain rule, we have

$$\frac{\partial E}{\partial w} = \frac{\partial E_u}{\partial u_{IEN}} \frac{\partial u_{IEN}}{\partial w} = -(u_{PID}) \frac{\partial u_{IEN}}{\partial w} \quad (6)$$

The selection of the suitable learning rate λ plays an important role in the convergence by adaptively adjusted online the weight-update. If the learning rate value is too small, it needs much time to obtain an acceptable solution. On the contrary, a large learning rate value will possibly lead to oscillation, preventing the error E_u to converge to zero.

For this reason, this part proposes a self-adaptive strategy for selecting the learning rate λ based on a Sugeno fuzzy logic. The input of the fuzzy model is the error E_u , and the derivative of error E_u , namely dE . The corresponding output is the learning rate λ . The Sugeno fuzzy model is constructed using the fuzzy rules shown in Table 1, where $z1=0$; $z2=5e^{-5}$ $z3=5e^{-4}$ and $z4=5e^{-3}$. The membership functions for fuzzy input variables are shown in Fig.4.

Table 1. Fuzzy rules table for scaling learning rate

$E_u \backslash dE$	LN	SN	Zero	SP	LP
LN	$z2$	$z3$	$z4$	$z4$	$z4$
SN	$z4$	$z3$	$z3$	$z3$	$z4$
Zero	$z3$	$z2$	$z1$	$z2$	$z3$
SP	$z4$	$z3$	$z3$	$z3$	$z4$
LP	$z4$	$z4$	$z4$	$z3$	$z2$

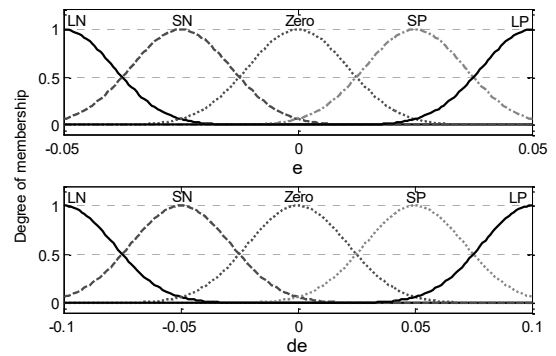


Fig. 4 Membership functions of the fuzzy input variables

2.3. Results and discussion

In this section, we study the performance and effectiveness of the proposed MFEL controller for a nonlinear system and its application to control the position of a shape memory alloy (SMA) actuator.

2.3.1. The benchmark nonlinear system

An original feedback error learning (FEL) controller approach is often tested on a robot arm system to validate the performance of FEL in [15], [18]–[20]. Therefore, in this test, the authors use the MFEL controller to control a 1-DOF arm robot model that is given as,

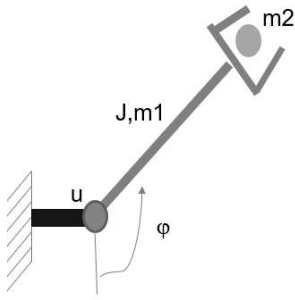


Fig. 5 1-DOF arm robot model

$$(m_1 l_c^2 + m_2 l^2) \ddot{\phi}(t) + J \dot{\phi}(t) + (m_1 l_c + m_2 l) g \sin \phi(t) = u(t) \quad (7)$$

Where, m_1 is a mass of arm. m_2 is a payload. l is a length of arm. l_c is a center of gravity position arm. J is a coefficient of friction. g is a gravity acceleration. $u(t)$ is the torque control as input signal. $\phi(t)$ is the end-effector position as an output signal. All parameters are set up as,

$$\ddot{\phi}(t) + 2\dot{\phi}(t) + 10 \sin \phi(t) = u(t) \quad (8)$$

a. Compensator based IEN model

Firstly, the benchmark system is implemented in Simulink with a sampling period of 0.1 seconds. Applying square waves with different amplitudes, the training data set and validating data set are collected and shown in Fig 6. Where, (a) use to estimate the model, (b) use to validate the IEN model.

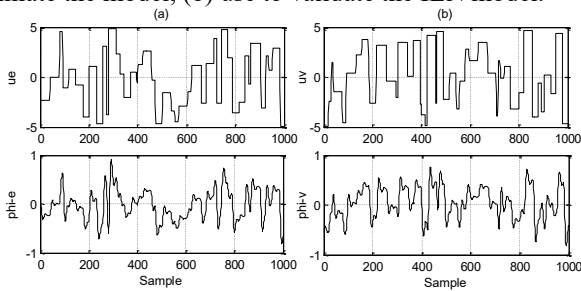


Fig. 6 Data for estimating and validating the IEN model

Secondly, the IEN model is used for identifying the dynamic of a nonlinear system in Eq.(7). The IEN structure is selected by 3-layer feedforward neural networks with S1 hidden neurons, S1 = 7; the number of generations GEN = 2000; number of populations NP = 62 and the 2nd order NARX structure.

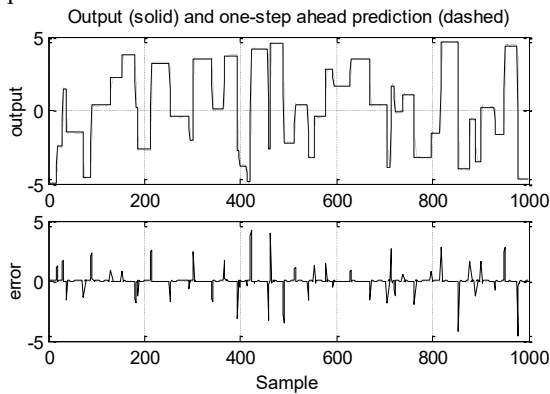


Fig.7 The identification performance of IEN model

Finally, the estimation and validation process is conducted to identify the IEN model. Fig.7 shows that the performance of identification inverse dynamic for the nonlinear system. The results demonstrate the better identification capability of the

IEN model. The final structure of the IEN model which includes a 3-layer with 4 inputs, 7 hidden nodes, and 1 output. The resulted weighting values of the IEN model precisely describe the nonlinear system which is used to generate the initial weight of the feedforward controller in the proposed MFEL controller.

b. Control results

The block diagram of the MFEL control approach applied to control of the nonlinear system in Eq.(7) is illustrated as Fig.8. The PID parameters are turned with the trial and error method and chosen to be $K_p = 80.2$ and $K_d = 20.5$.

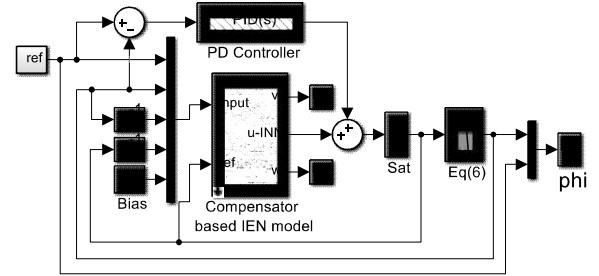


Fig.8 Block diagram of MFEL scheme in Simulink

Case study 1. In this case, the closed-loop performance is verified in changing the reference signal to survey the control performance of the controller. Fig.9 and Fig.10 compare the control performance of the proposed controller and the PID controller in two cases of sine and step without the payload, respectively. All these results show that the PID controller causes big error values. On the contrary, the proposed controller always adaptively minimizes the error value to converge to zero successfully.

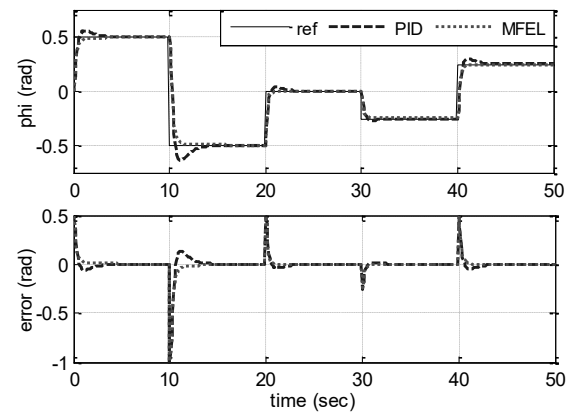


Fig.9 Quality control of Eq.(7) with step reference

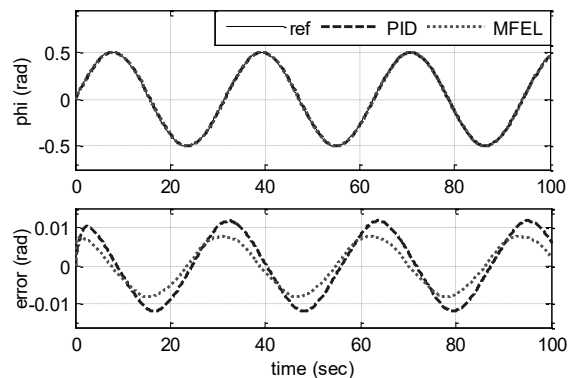


Fig.10 Quality control of Eq.(7) with sine reference

Fig.11 shows the control signal (u), where the output of the feedforward controller based on the IEN model (u_{IEN}), the component PID controller (u_{PID}), and the proposed MFEL controller (u_{MFEL}). dv/dt is the variation of the weights in the hidden layer of the IEN model. dw/dt is the variation of the weights in the output layer of the IEN model. After a finite time, the feedforward control based on the IEN model learns the inverse dynamics of the system and take the responsibility of the control system. Simultaneously, the output of the component PID controller tends to go to zero. Fig.11 also shows that the weights varied automatically during control operation in two cases of sine and step trajectory without payload, respectively.

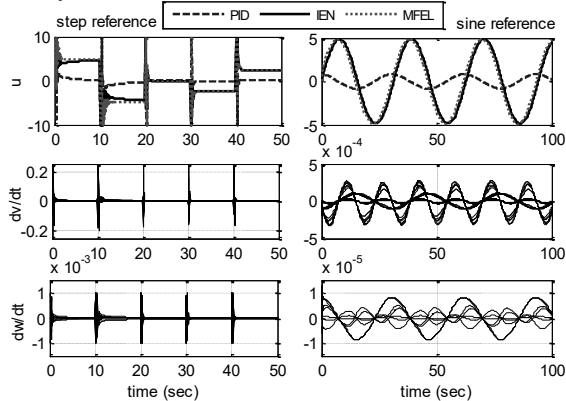


Fig.11 Online learning in control of Eq.(7)

Case study 2. Changing the payload of the nonlinear 1-DOF robot arm system in Eq.(7). Fig.12 shows the comparison results between the traditional PID controller and the proposed MFEL controller in two cases of sine and step trajectory with the payload, respectively.

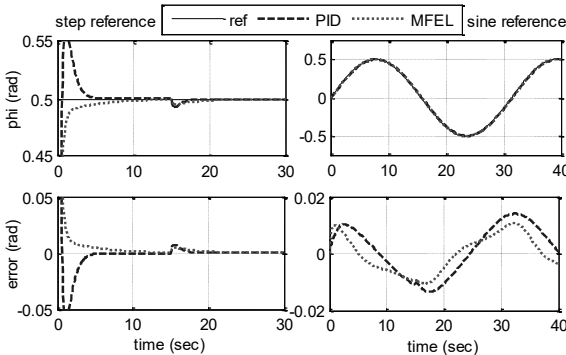


Fig.12 Quality control of Eq.(7) with payload

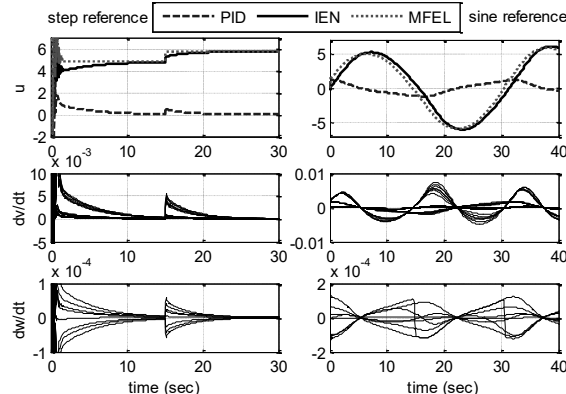


Fig.13 Online learning in control of Eq.(7) with payload

The figure shows that the performance of the MFEL controller is better than the PID controller. Fig.13 shows the overall control signal (u_{MFEL}), the output of the feedforward controller based on the IEN model (u_{IEN}) and the component PID controller (u_{PID}). Fig.13 also shows that the weights varied automatically during control operation in two cases of sine and step trajectory with payload, respectively.

Case study 3. Impacting the noise with $var=0.0001$, $mean=0$ and $T_s=0.5$ sec to the nonlinear system.

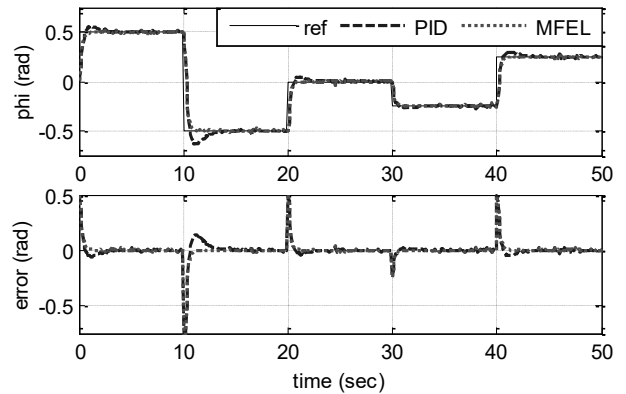


Fig.14 Quality control of Eq.(7) with noise

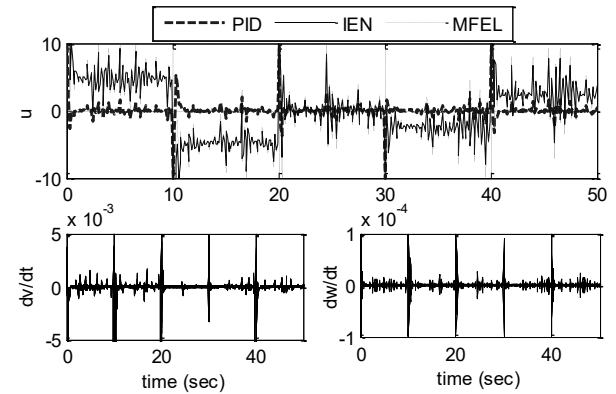


Fig.15 Online learning in control of Eq.(7) with noise

Fig.14 shows the comparison results between the traditional PID controller and the proposed MFEL controller in case of step trajectory. The figure shows that the performance of the MFEL controller is better than the PID controller. Fig.15 shows the overall control signal (u_{MFEL}), the output of the feedforward controller based on the IEN model (u_{IEN}) and the component PID controller (u_{PID}). Fig.15 also shows that the weights varied automatically during control.

In summary, the proposed modified feedback error learning (MFEL) control used the online auto-tuning capability of the aBP learning algorithm to accurately control the nonlinear SISO system. Based on the above results, we see that the proposed controller had an achieving stable high-performance control and the error between the reference signal and the output signal being optimized. The proposed controller had also strong adaptive ability and robustness in the presence of external disturbances and payload.

2.3.2. Applied in tracking control of SMA actuator

a. Configuration of SMA actuator system

An experimental SMA actuator architecture is shown as Fig.16. The experimental setup includes SMA spring, bias spring, power amplifier, rotary encoder, NI-PCI 6221 card, and a computer. The parameters of the SMA spring actuator are described in Table 2.

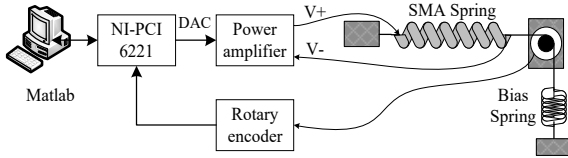


Fig.16 Diagram of the experimental SMA actuator

Table.2 Experimental device parameters

No	Devices	Parameters
1	SMA spring actuator	- Ni-Ti material, expansion spring - Wire diameter: 0.51 mm - Mean coil diameter: 6.0 mm - Generate force: 1.0 N
2	Rotary encoder	- Resolution(pulses/rotation): 500 - Power supply: 5V \pm 10%
3	NI-PCI 6221	- National Instrument Company. - Two 16-bit analog outputs (833 KS/s); 24 digital I/O; 32-bit counters - 16 Analog Inputs, 16-Bit, 250 KS/s.

When cool, the SMA actuator can be extended to 9cm. When heated, it contracts to 25mm overall. A power amplifier, which is controlled by digital to analog converter (or DAC) module of NI-PCI 6221 card, is applied SMA spring to heat. A bias spring is connected to the SMA spring to apply a restoring force. A rotary encoder is mounted to the spring to measure the displacement of SMA spring. This feedback signal is fed into the computer through an encoder module of NI-PCI 6221 card. The Real-Time Windows Target Toolbox of Matlab is used for the real-time control system.

b. Compensator based the IEN model

In this section, we find the IEN model to describe the hysteresis compensator of the SMA actuator. The procedure consists of four basic steps as follows,

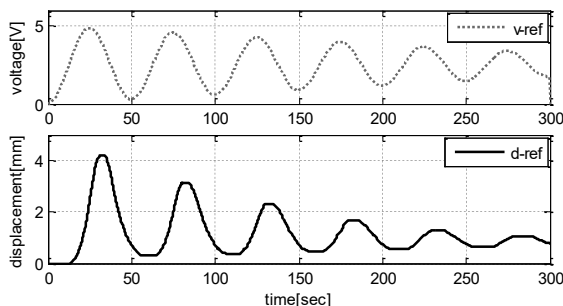


Fig.17 Data for estimation and validation purpose

Firstly, the SMA actuator system to generate a collection of experimental data relating the applied voltage input to the position output of the SMA actuator. Fig.17 shows applied voltage input (v-ref input) to the SMA actuator system and the responding position output collected. Voltage input and

position output from (0-150)[sec] are used for estimating the IEN model. Voltage input and position output from (150-300)[sec] are used for validating the IEN model.

Secondly, the IEN model is created by combining the 3-layer with 5 neurons of the hidden layer and the 2st order NARX model. Where the parameters of the MDE algorithm is selected as population size $NP = 50$, number of generations $GEN = 2000$.

Finally, the estimation and validation process is conducted to identify the IEN model. Fig.18 shows the performance based on the average values of MSE on the validating process. The result shows that the inverse model of the SMA actuator achieves good performance identification. These results will be used to provide for the compensator control.

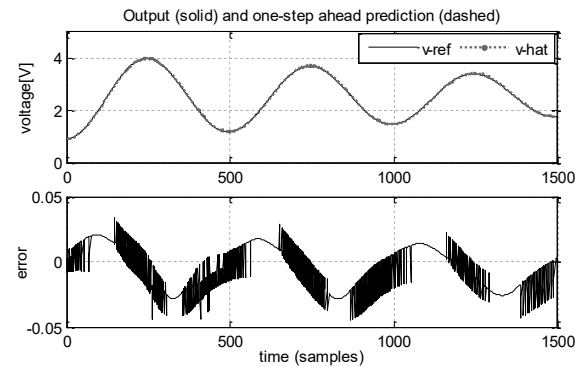


Fig.18 Performance on validating the IEN model

c. Experimental control results

The control programming is designed using the real-time window target of MATLAB. The PID parameters are chosen by trial and error method and determined to be $K_p = 7, K_i = 0, K_d = 7$.

Case study 1. Changing the reference signal to survey the position control performance of the SMA actuator. Fig.19 shows the performance of the proposed controller with sine reference and compares it to the PID controller. Fig.20 shows all control signals of the proposed controller. Based on the control results, we see that the proposed controller improves the quality significantly compared to the PID controller. And especially, the error learning in online updating to decrease to zero.

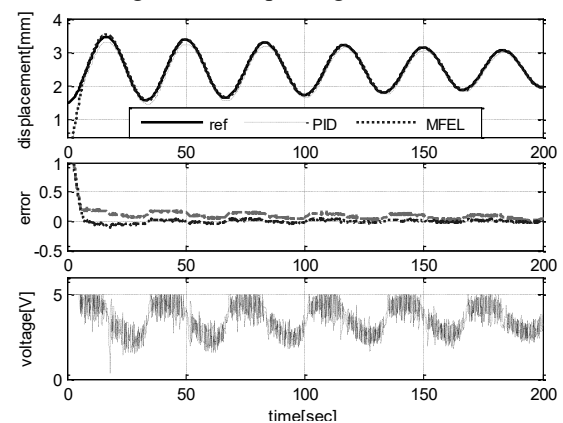


Fig.19 Quality control of SMA with sine reference

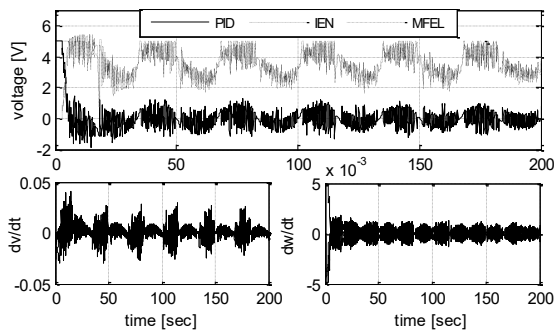


Fig.20 Online learning in control with sine reference

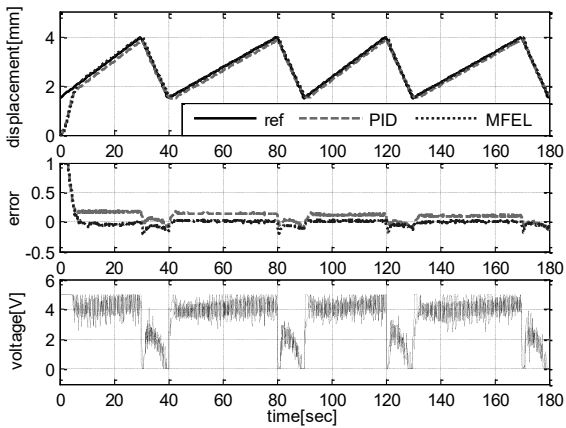


Fig.21 Quality control of SMA with triangle reference

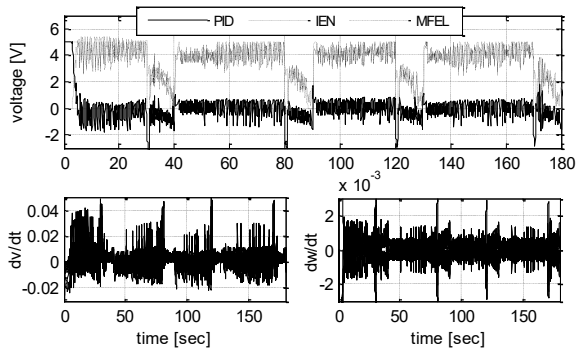


Fig.22 Online learning in control with triangle reference

Similarly, Fig.21 describes the quality of controlling the SMA actuator with a triangle trajectory. Figure 22 describes the output of the MFEL controller and the weight variations of the controller during the control. Based on the control results, we see that the MFEL control quality achieved good results despite changing the reference signal and achieving much better quality when compared to the PID controller. Adaptation of the MFEL controller is shown in the reduced control error while the PID controller does not improve the error in the control and the weights of the forward controller be updated online during control to improve control quality.

Case study 2: Changing the load by increasing the stiffness of spring bias to test the performance of the proposed controller. Figure 23 describes the quality control with the sine reference signal when changing the load at time $t = 90$ sec. Figure 24 describes the weighting variation of the MFEL controller during the control process.

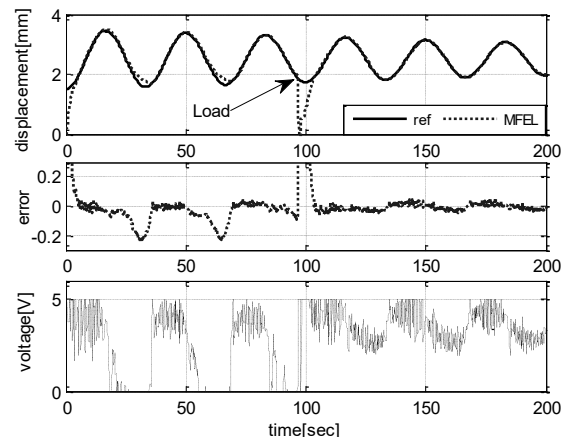


Fig.23 Quality control of SMA when changing load

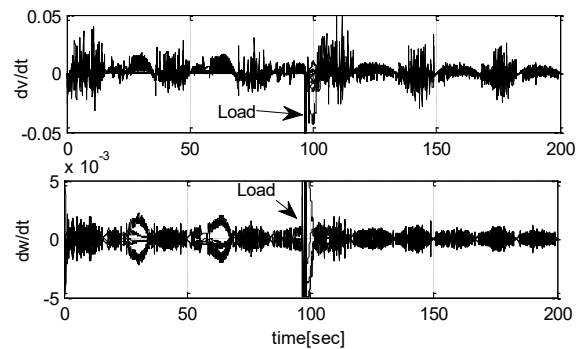


Fig.24 Online learning in control when changing load

The results show that the performance of the MFEL controller quite well. When changing the load at $t = 90$ sec, the weight values of INN is online updated to guarantee the quality control.

Case study 3: Generate the noise by impact to change the elasticity of bias spring or decrease the temperature of SMA by the fan and then do survey the quality control of the MFEL controller. Figure 25 shows the quality control with the sine reference signal when changing the noise.

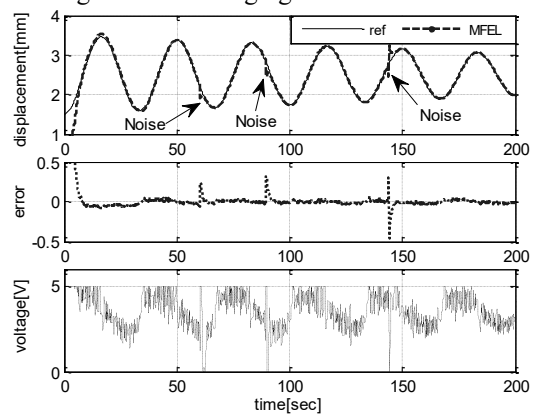


Fig.25 Quality control of SMA when changing noise

In summary, the proposed MFEL controller-based evolutionary neural network used the online auto-tuning capability of the aBP learning algorithm to accurately control of SMA actuator. Moreover, the proposed controller had also strong adaptive ability and robustness in the presence of external disturbances.

3. Conclusion

In this study, a modified feedback error learning (MFEL) control is developed and successfully applied to control the nonlinear SISO system. The MFEL controller is modified from the original FEL version by adding an evolutionary neural network and an adaptive back-propagation (aBP) with a self-adaptive learning rate using the Sugeno Fuzzy model. The simulation on the benchmark nonlinear system is firstly tested to evaluate the performance of the MFEL controller. Then, the proposed controller is applied to position control of the SMA actuator. Experimental results prove that the proposed MFEL controller can learn and update the inverse hysteresis of the SMA actuator to reduce the tracking error to nearly zero. Future works will study to implement the proposed MFEL controller for other hysteresis nonlinear systems.

Acknowledgement

This research is funded by Vietnam National Foundation for Science and Technology Development (NAFOSTED) under grant number 107.01-2018.318.

References

- [1] L. G. Machado and M. A. Savi, "Medical applications of shape memory alloys," *Brazilian J. Med. Biol. Res.*, vol. 36, no. 6, pp. 683–691, 2003.
- [2] C. Majidi, "Soft robotics: a perspective—current trends and prospects for the future," *Soft Robot.*, vol. 1, no. 1, pp. 5–11, 2014.
- [3] Y. Liu, H. Du, L. Liu, and J. Leng, "Shape memory polymers and their composites in aerospace applications: a review," *Smart Mater. Struct.*, vol. 23, no. 2, p. 23001, 2014.
- [4] M. Al Janaideh, S. Rakheja, and C.-Y. Su, "An analytical generalized Prandtl–Ishlinskii model inversion for hysteresis compensation in micropositioning control," *IEEE/ASME Trans. mechatronics*, vol. 16, no. 4, pp. 734–744, 2011.
- [5] R. V. Iyer, X. Tan, and P. S. Krishnaprasad, "Approximate inversion of the Preisach hysteresis operator with application to control of smart actuators," *IEEE Trans. Automat. Contr.*, vol. 50, no. 6, pp. 798–810, 2005.
- [6] M. Zhou, S. He, Q. Zhang, K. Ji, and B. Hu, "Hybrid control of magnetically controlled shape memory alloy actuator based on Krasnosel'skii–Pokrovskii model," *J. Intell. Fuzzy Syst.*, vol. 29, no. 1, pp. 63–73, 2015.
- [7] J.-H. Lin and M.-H. Chiang, "Tracking Control of a Magnetic Shape Memory Actuator Using an Inverse Preisach Model with Modified Fuzzy Sliding Mode Control," *Sensors*, vol. 16, no. 9, p. 1368, 2016.
- [8] C. Xiang *et al.*, "The design, hysteresis modeling and control of a novel SMA-fishing-line actuator," *Smart Mater. Struct.*, vol. 26, no. 3, p. 37004, 2017.
- [9] A. U. Awan, J. Park, H. J. Kim, J. Ryu, and M. Cho, "Adaptive control of a shape memory alloy actuator using neural-network feedforward and RISE feedback," *Int. J. Precis. Eng. Manuf.*, vol. 17, no. 4, pp. 409–418, 2016.
- [10] M. Zhou and Q. Zhang, "Hysteresis model of magnetically controlled shape memory alloy based on a PID neural network," *IEEE Trans. Magn.*, vol. 51, no. 11, pp. 1–4, 2015.
- [11] N. Nikdel, P. Nikdel, M. A. Badamchizadeh, and I. Hassanzadeh, "Using neural network model predictive control for controlling shape memory alloy-based manipulator," *IEEE Trans. Ind. Electron.*, vol. 61, no. 3, pp. 1394–1401, 2014.
- [12] M. R. Zakerzadeh and H. Sayyaadi, "Precise position control of shape memory alloy actuator using inverse hysteresis model and model reference adaptive control system," *Mechatronics*, vol. 23, no. 8, pp. 1150–1162, 2013.
- [13] S. N. Nguyen, V. Ho-Huu, and A. P. H. Ho, "A neural differential evolution identification approach to nonlinear systems and modelling of shape memory alloy actuator," *Asian J. Control*, vol. 20, no. 1, pp. 57–70, 2018.
- [14] M. Kawato, "Feedback-error-learning neural network for supervised motor learning," *Adv. neural Comput.*, vol. 6, no. 3, pp. 365–372, 1990.
- [15] H. Miyamoto, M. Kawato, T. Setoyama, and R. Suzuki, "Feedback-error-learning neural network for trajectory control of a robotic manipulator," *Neural networks*, vol. 1, no. 3, pp. 251–265, 1988.
- [16] K. S. Narendra and A. M. Annaswamy, *Stable adaptive systems*. Courier Corporation, 2012.
- [17] J. Nakanishi and S. Schaal, "Feedback error learning and nonlinear adaptive control," *Neural Networks*, vol. 17, no. 10, pp. 1453–1465, 2004.
- [18] K. Kurosawa, R. Futami, T. Watanabe, and N. Hoshimiya, "Joint angle control by FES using a feedback error learning controller," *IEEE Trans. Neural Syst. Rehabil. Eng.*, vol. 13, no. 3, pp. 359–371, 2005.
- [19] K. Sabahi, S. Ghaemi, and M. A. Badamchizadeh, "Feedback error learning-based type-2 fuzzy neural network predictive controller for a class of nonlinear input delay systems," *Trans. Inst. Meas. Control*, p. 0142331219834998, 2019.
- [20] X. Ruan, M. Ding, D. Gong, and J. Qiao, "On-line adaptive control for inverted pendulum balancing based on feedback-error-learning," *Neurocomputing*, vol. 70, no. 4–6, pp. 770–776, 2007.